

DESIGN OF 35 GHz GYROTRON FOR MATERIAL PROCESSING APPLICATIONS

N. Kumar [†], U. Singh, A. Kumar, and H. Khatun

Gyrotron Laboratory, Microwave Tube Area
Central Electronics Engineering Research Institute (CEERI)
Council of Scientific and Industrial Research, CSIR
Pilani, Rajasthan 333031, India

T. Singh

Department of Physics, JV College, Baraut, UP, India

A. Sinha

Gyrotron Laboratory, Microwave Tube Area
Central Electronics Engineering Research Institute (CEERI)
Council of Scientific and Industrial Research, CSIR
Pilani, Rajasthan 333031, India

Abstract—The complete design of 35 GHz, 200 kW gyrotron for various material processing and heating applications is presented in this article. The components of the device, such as Magnetron Injection Gun, interaction cavity, collector and RF window, are designed for the TE₀₃ mode. Various in-house developed codes (GCOMS, MIGSYN and MIGANS) and commercially available codes (MAGIC, EGUN and CST-MS) are used for the design purpose. A thorough sensitivity analysis of the gyrotron components is also carried out. The designed device shows the capability to generate more than 200 kW of output power with more than 40% of efficiency.

1. INTRODUCTION

The gyrotron is a microwave vacuum device, capable to generate hundreds of kilowatts of electromagnetic power in the millimeter

Received 2 November 2010, Accepted 9 December 2010, Scheduled 15 December 2010

Corresponding author: Nitin Kumar (nitin.physika@rediffmail.com).

[†] Also with Department of Physics, JV College, Baraut, UP, India.

and sub-millimeter wave spectrum [1, 2]. The device is based on the phenomena called Cyclotron Resonance Maser (CRM) instability occurring during the interaction of the helically moving electrons and RF [3]. The development of the gyrotron device was initiated by the plasma physics community due to the requirement of high power millimeter wave radiation source in the Electron Cyclotron Resonance Heating (ECRH) of magnetically confined plasma [4]. At the present time, the gyrotron is a signature device for the plasma fusion applications and expanding its influence in the other areas of science and technology, like, material processing, THz spectroscopy, atmospheric analysis etc due to various inherent advantages of millimeter/submillimeter wave radiation over microwave radiation [5, 6]. The uniform and the localized heating are the main advantages of millimeter wave radiation in the material processing and heating [7]. Due to the short wavelength, the millimeter wave radiation can be focused as a pencil beam and is used in the surface treatment of materials [8]. Considering all these advantages, the gyrotrons of low frequency ranges in the millimeter wave spectrum are used in material processing applications [9–11]. The millimeter wave frequencies of 24 GHz and 28 GHz have been investigated widely for the material processing applications by the gyrotron community [11–13]. 35 GHz is also a popular frequency in the millimeter wave region due to the natural atmospheric window at this frequency and thus used in the communication and whether diagnosis applications [14, 15]. Some research groups have worked on this frequency to utilize it in the material processing applications [16, 17], but still 24 and 28 are much popular. *Fliflet et al.* has been designed and used the gyrotron operating at TE_{01} mode with the output power of 30–100 kW in the material processing application [16]. *Barroso et al.* has also been presented the conceptual design and the experimental results of the 35 GHz gyrotron operating at TE_{02} mode and producing 100 kW of output power [18]. It is planned to establish a material processing (ceramic sintering) unit based on 35 GHz millimeter wave heating to investigate the advantages or disadvantages of this frequency (like densification, grain size, fast heating) in the material processing in more detail. The gyrotron as a 35 GHz radiation source is the most important component of this material processing unit.

In this paper, the detail design of 35 GHz gyrotron vacuum tube operating at first harmonic for the material heating and processing applications is presented. The schematic diagram of the gyrotron is shown in Figure 1 with the description of different components. The different components of the gyrotron will be joined together by various techniques like brazing, flanges, TIG welding, etc. The axial coupling

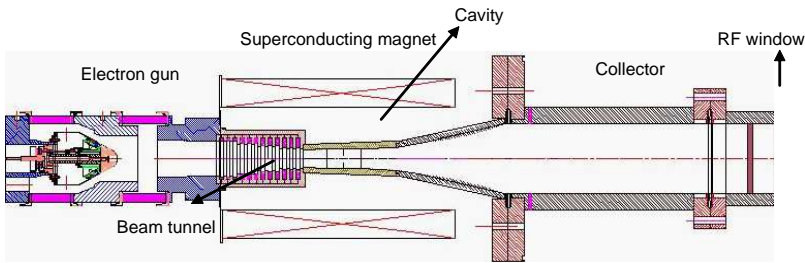


Figure 1. Schematic diagram of 35 GHz gyrotron.

Table 1. The design goal of the gyrotron.

Frequency (f)	35 GHz
Output power (P_{out})	≥ 200 kW
Efficiency (η)	$\geq 35\%$
Beam voltage (V_b)	65 kV
Beam current (I_b)	10 A
Wall loss	< 1 kW/cm ²
Voltage Depression (V_d)	$< 10\%$ of V_b

is chosen in the 35 GHz gyrotron just due to simplicity, although the radial power extraction is better than the axial power extraction due to its various advantages like the internal mode conversion of the operating mode into Gaussian mode, the better separation of RF power from the electron beam, etc. The design goals for the 35 GHz gyrotron are summarized in Table 1. To design the various components of gyrotron like electron gun, magnet system, interaction cavity, beam collector, RF window, the various in house developed and commercially available computer codes are used. The design study of 35 GHz gyrotron proves more than 200 kW of output power at 40% of interaction efficiency.

2. MODE SELECTION AND COLD CAVITY ANALYSIS

The various low order TE modes are studied carefully by using the computer code GCOMS to fulfill the gyrotron design goals. Finally, symmetric TE₀₃ mode is selected as the operating mode on the basis of various mode selection parameters, like, the space charge effect and the ohmic wall loading [19–21]. The cavity radius (R_c) and the beam radius (R_b) for the second radial maxima are calculated on the basis of selected operating mode. The middle section length (L) of the

Table 2. Frequency and Q factor with respect to cavity middle section length.

Middle section length (L) in mm	Frequency (f) in GHz	Quality factor (Q)
40	34.916	416
42	34.912	458
44	34.900	503
46	34.902	550
48	34.896	600
50	34.894	650
52	34.889	703

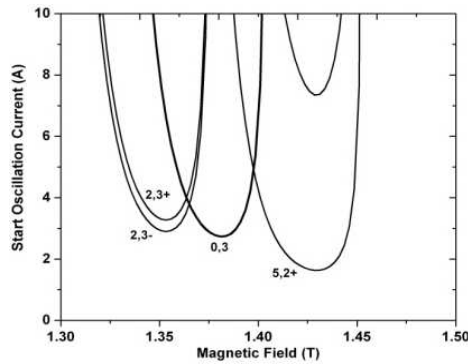


Figure 2. Start oscillation current curves with respect to the cavity magnetic field.

interaction cavity is optimized on the basis of diffractive quality factor calculations ($5\lambda \leq L \leq 7\lambda$) shown in Table 2. Finally, 46 mm is chosen as the interaction cavity middle section length. The ohmic wall loss for the calculated dimensions of the interaction cavity is quite below the limit as described in the Table 1. The input and the output taper section geometries are optimized by using electromagnetic simulation tool MAGIC based on the Particle-in-Cell numerical approach [22]. To analyze the mode competition in the interaction cavity, the Start Oscillation Current (SOC) is studied. Figure 2 shows the SOC of various competing modes including operating mode TE_{03} . $TE_{2,3}$ is the most competing mode as it shows approximately the same start-up condition. Overall, TE_{03} mode is well separated from the neighboring modes.

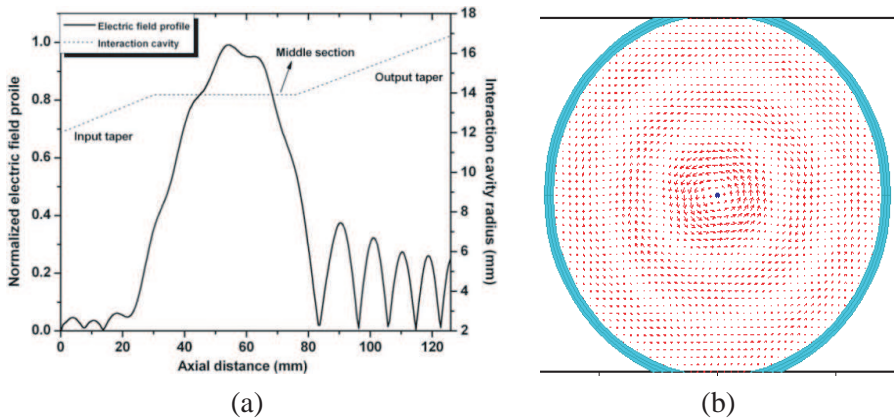


Figure 3. (a) Normalized axial electric field profile in the interaction cavity. (b) TE_{03} mode pattern in the interaction cavity at 34.9 GHz of resonant frequency.

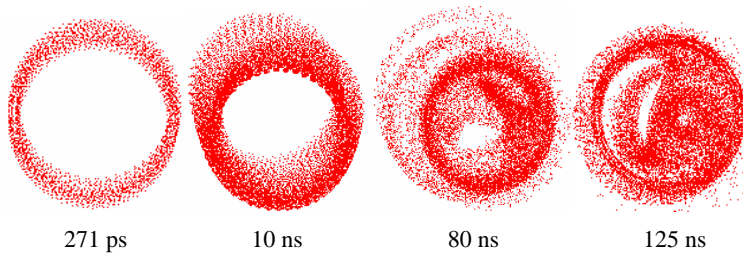


Figure 4. Time evolution process of the electron beam phase during the beam-wave interaction.

Figure 3 shows the cold cavity results obtained by the MAGIC simulations. The normalized axial electric field profile with the interaction cavity geometry and the operating mode pattern are shown in Figures 3(a) and 3(b), respectively. The maximum electric field strength is at the center of the cavity and indicates the standing wave profile. In the output taper section, the RF field profile is like a traveling wave, which is required for the efficient power extraction from the middle section of the cavity.

3. BEAM-WAVE INTERACTION COMPUTATION

The beam-wave interaction takes place at the middle section of the interaction cavity. The gyrating electron beam, emitted from the

triode-type electron gun (discussed in next section in detail), launched at the entrance of input taper section for the interaction. The same electron beam interact with the RF, present in the cavity in the form of TE_{03} mode, and get collected in the specially designed circular type of waveguide called collector (discussed in next sections). To maintain sufficient beam-metal wall gap, the electron beam is launched at the second radial maxima of the TE_{03} mode. MAGIC code is used for the beam-wave interaction and efficiency computations.

Figure 4 shows the evolution process of the electron beam phase bunching with respect to time. As the electromagnetic wave energy grows in time, the electrons bunched more effectively in phase within their cyclotron orbit. At 125 ns (stability time), the electrons bunched very tightly, which indicates the efficient power is transferred to the

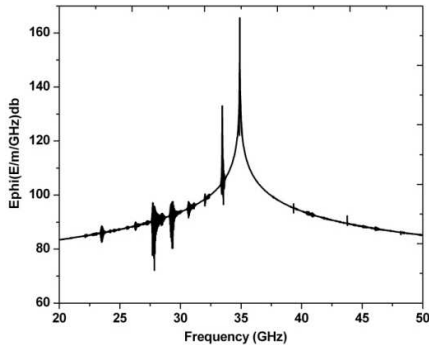


Figure 5. Frequency spectrum in the interaction cavity.

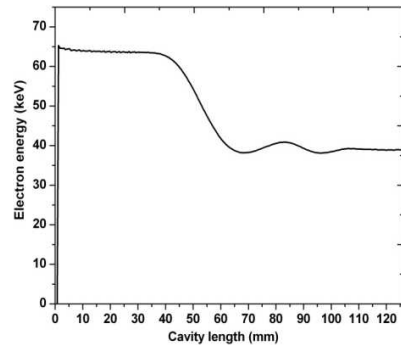


Figure 6. Electron energy profile in the interaction cavity.

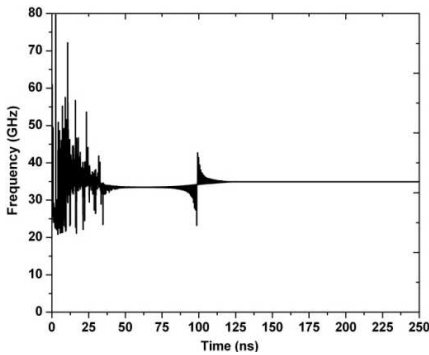


Figure 7. Frequency growth with respect to time.

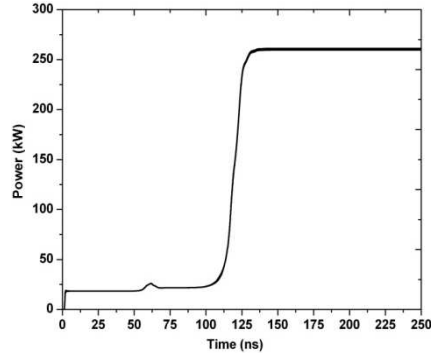


Figure 8. Power growth with respect to time.

RF. Figures 5 to 8 show the beam-wave interaction simulations results. The frequency spectrum and the electron energy profile indicate the stable oscillation of the operating mode and energy transfer mechanism in the interaction cavity, respectively. The peak of gain in electric field occurs at 34.9 GHz of frequency and surrounding of this peak, other oscillations are suppressed completely. This indicates the power growth in TE_{03} mode because 34.9 GHz is the calculated resonant frequency of the operating mode. The energy profile curve shows the maximum energy transfer occurs at the middle of interaction cavity, which is identical to the axial electric field profile as shown in Figure 3(a). Figures 7 and 8 show the frequency and RF power growth in the cavity. Some kind of noise oscillations takes place in the cavity up to 125 ns and after this time, the stability occurs in the power and the frequency growth. Finally, 260 kW of output power is generated in the cavity at 1.34 T of cavity magnetic field with 40% of interaction efficiency. The optimized interaction cavity parameters are summarized in Table 3.

The interaction cavity parametric analysis is shown in Figure 9. The variation in the oscillation frequency is very small with respect to beam current, beam voltage, magnetic field and electron beam velocity ratio. The output power increases linearly with the beam voltage, while the efficiency reduces with respect to the beam current because of the space charge effect. The output power reduces approximately linearly with cavity magnetic field. At the magnetic field of 1.33 T, the output power and the operating frequency reduce drastically. The operating mode is disappeared below the critical value of the cavity magnetic field

Table 3. Final interaction cavity parameters.

Middle section length (L)	46 mm
Input taper length (L_1)	30 mm
Output taper length (L_2)	52 mm
Cavity radius (R_c)	13.9 mm
Input taper angle (θ_1)	3.5°
Output taper angle (θ_2)	3.5°
Beam radius (R_b)	7.27 mm
Velocity ratio of electron beam (α)	1.4
Beam current (I_b)	10 A
Beam voltage (V_b)	65 kV
Operating mode	$TE_{0,3}$
Quality factor (Q)	550
Cavity magnetic field	1.34 T

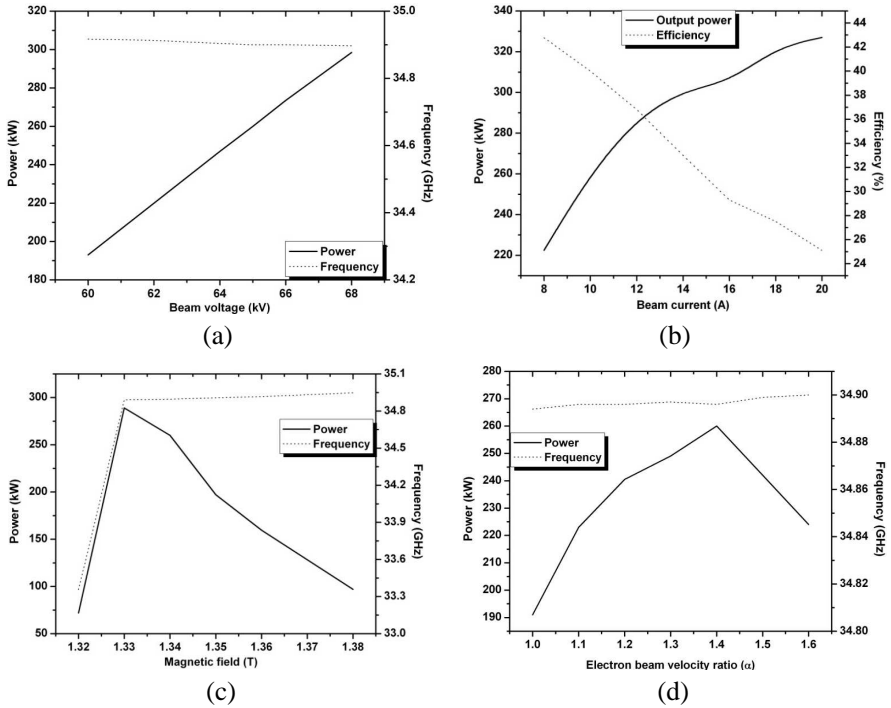


Figure 9. Interaction cavity parametric analysis. (a) Power and frequency v/s beam voltage. (b) Power and efficiency v/s beam current. (c) Power and frequency v/s magnetic field. (d) Power and frequency v/s Electron beam velocity ratio.

1.33 T and some other mode comes into picture. The critical limit of detuned magnetic field is 1.33 T. The electron beam velocity ratio is a very important beam parameter and plays the major role in the power growth mechanism in the cavity. The peak output power is achieved at $\alpha = 1.4$ as shown in Figure 9(d).

4. MAGNET SYSTEM

In the present design, the magnet system consists of two independent magnet coils, one is superconducting coil and other is gun coil. Some other magnet coils are also used at the collector region for the efficient electron beam spreading, discussed in the Section 6. The superconducting coil mainly determines the magnetic field at the interaction cavity region. The gun coil is placed above the emitter

and mainly controls the magnetic field distribution in the gun region for the efficient emission and formation of electron beam. The final optimized magnetic field profile is shown in Figure 10.

5. ELECTRON GUN

The triode-type magnetron injection gun (MIG) is used as the gyrating electron beam source. A 650 kW MIG is designed for the 35 GHz gyrotron tube. Two design goals are considered in the MIG design i.e., high transverse velocity of electrons and minimum velocity spread. The initial MIG parameters which are essential for the modeling

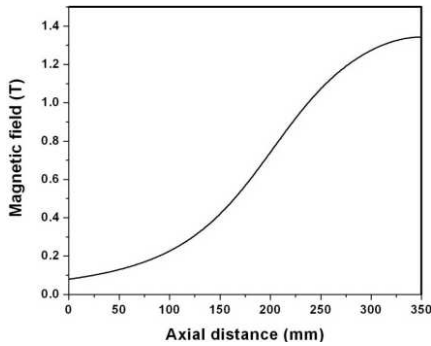


Figure 10. The optimized magnetic field profile.

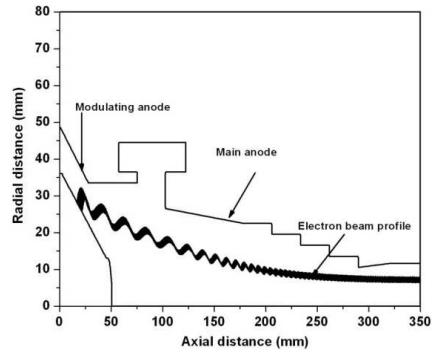


Figure 11. The designed MIG with electron beam profile and electrode geometry.

Table 4. The optimized electron beam and MIG geometry parameters.

Cathode magnetic field (B_{zc})	952.9 Gauss
Cavity magnetic field (B_0)	1.34 T
Average beam radius Beam radius (r_b)	7.25 mm
Velocity ratio (α)	1.39
Velocity spread ($\delta\beta_{\perp \max}$)	3.48%
Larmour radius (r_l)	0.529 mm
Cathode radius (r_c)	27.15 mm
Cathode slant length (l_s)	3 mm
Cathode current densit (J_c)	1 A/cm ²
Normalized perpendicular electron velocity (v_{\perp})	0.37
Modulating anode voltage	29 kV

and the electron trajectory simulations are obtained by using the analytical tradeoff equations [23–25]. The commercially available electron trajectory code EGUN [26] and two in-house developed code MIGSYN and MIGANS [23, 27] are used for the MIG design optimization. MIGANS is basically a post processor of the EGUN code and is used to find out the different electron beam parameters like electron beam velocity ratio, the average transverse velocity spread, the larmor radius (r_l), etc. Considering the technical limits, first the shape of the electrodes including the emitter is optimized for the low transverse velocity spread at the nominal beam parameters and then the electron beam parameters at the interaction cavity are optimized. The numerical calculations are performed in EGUN with 32 beamlets. The optimized values of the modulating anode voltage and the accelerating anode voltage are 29 kV and 65 kV, respectively with 10 A of beam current. Figure 11 shows the optimized geometry of the MIG with the electron beam profile and the shapes of electrodes obtained by the EGUN simulations. The optimized values of the electron beam parameters by using EGUN are summarized in Table 4.

Figure 12 shows the sensitivity analysis of the electron beam quality parameters (α and $\delta\beta_{\perp\max}$) with respect to the cathode magnetic field and the modulating anode voltage. The quality parameters vary approximately linearly with respect to the cathode magnetic field and modulating anode voltage.

6. BEAM TUNNEL

The beam tunnel is a lossy waveguide type of structure, used in the gyrotron to absorb the backward RF propagation towards the electron gun [19]. The structure is made of the periodic arrangement of the lossy ceramic rings and the OFHC (Oxygen Free High Conductivity) copper rings. The design of the beam tunnel is based on the methodology described in detail elsewhere [28]. The spurious oscillations are the major problem in the design of beam tunnel and a thorough analysis of these kinds of oscillations is very necessary. The excitation of the oscillations degrades the electron beam quality, which again affects the beam-wave interaction in the interaction cavity and output power performance. A detail analysis of the spurious oscillations in the beam tunnel is described by *Gantenbien et al.* [29]. The similar geometry of the beam tunnel is used in this gyrotron as described in [28]. The lossy ceramic AlN-SiC is used in the 35 GHz beam tunnel to absorb the backward RF propagation and to suppress the spurious mode oscillations. The dielectric properties of AlN-SiC are summarized in Table 5.

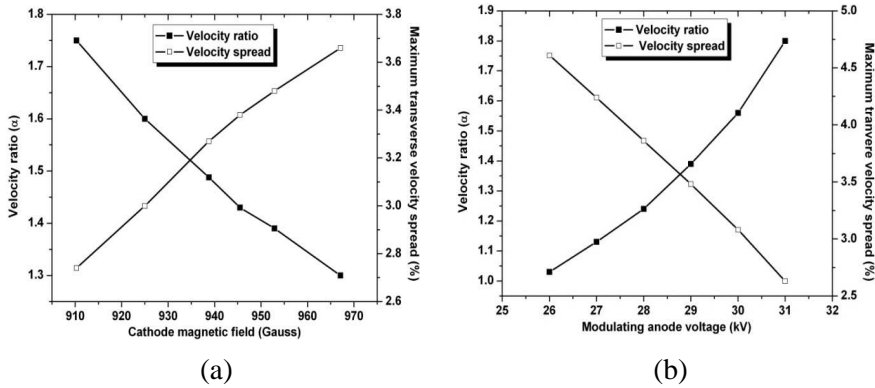


Figure 12. Sensitivity analysis of electron beam quality parameters i.e., Velocity ratio and transverse velocity spread v/s. (a) Cathode magnetic field. (b) Modulating anode voltage.

Table 5. Properties of lossy ceramic material.

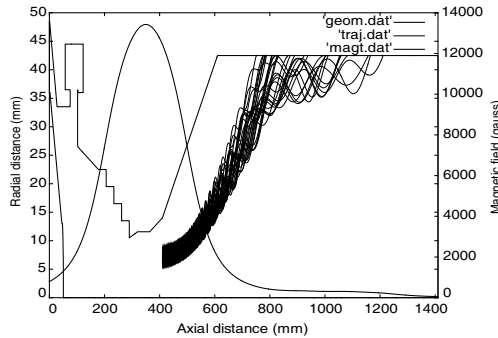
Loss Tangent ($\tan \delta$)	15
Relative Permittivity (ϵ_r)	0.25
composition	40 wt%SiC

7. BEAM DUMPING SYSTEM

The un-depressed collector is designed for the 35 GHz gyrotron due to its easy fabrication. The EGUN code is used for the collector design [30, 31]. Approximately 60% of the electron beam energy after the beam-wave interaction is dissipated on the collector wall. The length and the radius of the collector have been optimized by the analysis of the electron trajectory through EGUN simulation so that the maximum beam spread can be obtained. The maximum electron beam spreading reduces the heat loading at the collector wall which again makes the thermal management of the collector much easy. Three extra collector magnet coils are used to spread out the electron beam. The position and the magnetic field strength data of the coils are summarized in the Table 6. Figure 13 shows the magnetic field and electron beam profile with the optimized collector length and radius. The maximum achieved electron beam spread at the collector surface is 440 mm. At this beam spread, the heat dissipation at the collector wall is 0.35 kW/cm², which is sufficient below the critical limit (2 kW/cm²).

Table 6. The collector magnet coils data.

Magnet coils	Position		Magnetic field strength (Gauss)
	Axial	Radial	
Magnet A	800 mm	140 mm	370
Magnet B	900 mm	140 mm	350
Magnet C	975 mm	140 mm	245

**Figure 13.** Electron trajectories with the optimized collector geometry.

8. RF WINDOW

The RF window is a very critical part of any gyrotron tube. This system separates the ultrahigh vacuum environment inside the tube ($> 10^{-7}$ torr) from the external system located in the normal pressure environment. Due to the separation of two very opposite environments, the window material must be very good in case of mechanical strength and pressure gradient. Ideally, the generated RF power should be transmitted through the window material without any reflection and absorption. Considering all these aspects, various kinds of dielectric materials like sapphire, SiN, CVD diamond, BN, Au doped Silicon, etc. have been studied by various research groups to fulfill the mechanical, thermal and electrical properties required in the design of high power RF window [1, 32, 33]. In this design study, CVD diamond material is selected as the window material due to its very good mechanical and electrical properties summarized in Table 7. The CVD diamond also provides good compatibility with the brazing and metallization process. Due to the very good thermal conductivity of CVD diamond and very weak dependency of the electrical parameters on temperature, edge cooled single disk design is selected for this gyrotron.

Table 7. Window material properties [27].

Permittivity	5.6
Los tangent	10^{-5}
Thermal conductivity	10000

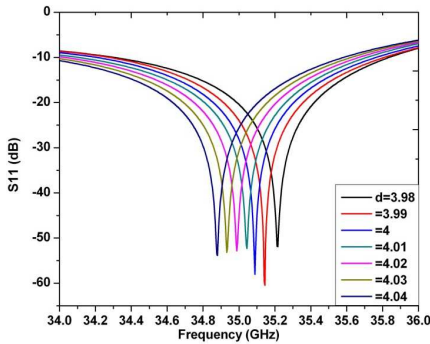


Figure 14. Reflection characteristic of RF window for different disk thickness.

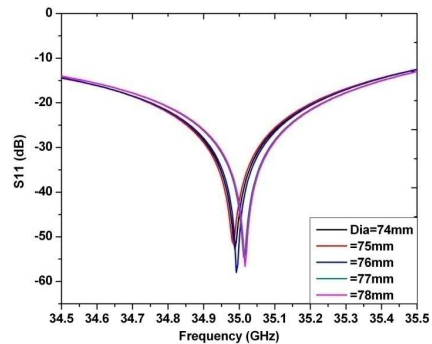


Figure 15. Reflection characteristic for different disk diameter.

The diamond disk thickness and the diameter are optimized by considering the Gaussian beam profile in the window design. The reflection parameter with respect to various disk thicknesses and diameters is shown in Figures 14 and 15. The CST-Microwave Studio (CST-MS) electromagnetic simulator is used for the simulations [34]. Finally, 76 mm of disk diameter and 4.02 mm of disk thickness ($d = n\lambda/2\epsilon_r^{1/2}$, λ is the free space wavelength and ϵ_r is the permittivity of window material) is chosen on the basis of minimum reflection and absorption of the RF power.

9. CONCLUSION

The presented study shows the design feasibility and detail analysis of various components of 35 GHz, 200 kW gyrotron operating at TE₀₃ mode. The simulation results show 260 kW of output power at 34.9 GHz of resonance frequency and 1.34 T of cavity magnetic field. On the basis of the decided design goals, a 650 kW of MIG is designed with the electron velocity ratio of 1.4 and transverse velocity spread of 3.48%. The un-depressed collector is designed considering the 40% of interaction efficiency (by cavity simulation results) and the very good

electron beam spread (440 mm) at the collector wall is achieved. The CVD diamond is used as the RF window material due to its excellent thermal, dielectric and mechanical properties. The rigorous parametric study of the components is also done, which will be helpful in the actual fabrication of the device.

ACKNOWLEDGMENT

The authors are pleased to acknowledge the support of Dr. Chandra Shekhar, Director, CEERI Pilani and Dr. SN Joshi, National Coordinator of Gyrotron project. The authors also wish to thank the team members of gyrotron for helpful discussions. Thanks are also due to Council of Scientific and Industrial Research (CSIR) for awarding the Senior Research Fellowship to Mr. Nitin Kumar.

REFERENCES

1. Thumm, M., "State-of-the-art of high power gyro-devices and free electron masers update 2004," FZK, KIT, Germany.
2. Thumm, M., "Progress in gyrotron development," *Fusion Engineering and Design*, Vol. 66–68, 69–90, 2003.
3. Flyagin, V. A., A. V. Gaponov, I. Petelin, and V. K. Yulpatov, "The gyrotron," *IEEE Trans. Microwave Theory. Tech.*, Vol. 25, 514–521, 1977.
4. Thumm, M., "MW gyrotron development for fusion plasma applications," *Plasma Physics and Controlled Fusion*, Vol. 45, A143, 2003.
5. Thumm, M., "Novel applications of millimeter and submillimeter wave gyro-devices" *Int. J. of Infrared, Millimeter and Terahertz Wave*, Vol. 22, 377–386, 2001.
6. Gold, S. H. and G. S. Nusinovich, "Review of high-power microwave source research," *Rev. Sci. Instrum*, Vol. 68, 3945–3974, 1997.
7. Hirota, M., M. C. Valecillo, M. E. Britoc, K. Hiraob, and M. Toriyamad, "Grain growth in millimeter wave sintered silicon nitride ceramics," *Journal of the European Ceramic Society*, Vol. 24, 3337–3343, 2004.
8. Bykov, Y. V., A. G. Eremeev, V. V. Holoptsev, K. I. Rybakov, and V. E. Semenov, "High temperature processing of materials using millimeter-wave radiation," *Proc. MSMW Symposium*, Kharkov, Ukraine, 1998.

9. Felich, K. L., et al., "Characteristics and applications of fast-wave gyro-devices," *Proceeding of the IEEE*, Vol. 87, 752, 1999.
10. Miyake, S., "Millimeter-wave materials processing in Japan by high-power gyrotron," *IEEE Trans. Plasma Sci.*, Vol. 31, 1010–1015, 2003.
11. Toshiyuki, Y. M., T. Matsumoto, and S. Miyake, "Fabrication of bulk ceramics by high power millimeter wave radiation," *Japanese J. Applied Physics*, Vol. 40, 1080–1082, 2001.
12. Liu, P.-K., E. Borie, and M. V. Kartikeyan, "Design of a 24 GHz, 25–50 kW Technology gyrotron operating at the second harmonic," *Int. J. Infrared Milli. Waves*, Vol. 21, 1917–1943, 2000.
13. Bykov, Y., G. Denisov, A. G. Ereemeev, M. Glyavin, V. V. Holoptsev, I. V. Plotnikov, and V. Pavlov, "3.5 kW 24 GHz compact gyrotron system for microwave processing of materials," *Advances in Microwave and Radio Frequency Processing*, Part 1, 24–30, 2006.
14. Liebe, H. J., "MPM — an atmospheric millimetre-wave propagation model," *Int. J. Infrared Milli. Waves*, Vol. 10, 631–650, 1989.
15. Gaponov-Grekhov, A. V. and V. L. Granatstein, *Application of High Power Microwaves*, Artech House Publication, London, 1994.
16. Fliflet, A. W., et al., "Sintering of ceramic compacts in a 35 GHz gyrotron-powered furnace," *Proc. IEEE Int. Conf. on Plasma Science*, 159–160, San Diego, USA, 1997.
17. Fliflet, A. W., et al., "Pulsed 35 GHz gyrotron with overmoded applicator for sintering ceramic compacts," *Proc. IEEE Int. Conf. on Plasma Science*, 105–106, Boston, USA, 1996.
18. Barroso, J. J., A. Montes, G. O. Ludwig, and R. A. Correa, "Design of a 35 GHz gyrotron," *Int. J. Infrared Milli. Waves*, Vol. 11, 251–274, 1990.
19. Edgcombe, C. J., Ed., *Gyrotron Oscillators: Their Principles and Practice*, Taylor & Francis, London 1993.
20. Gantenbein, G., E. Borie, O. Dumbrajs, and M. Thumm, "Design of a high order volume mode cavity for a 1 MW/140 GHz gyrotron," *Int. J. Electronics*, Vol. 78, 771–787, 1995.
21. Jain, R. and M. V. Kartikeyan, "Design of a 60 GHz, 100 kW CW gyrotron for plasma diagnostics: GDS-V.01 simulations," *Progress In Electromagnetics Research B*, Vol. 22, 379–399, 2010.
22. MAGIC User Manual: 2007 version of Magic 3D, ATK Mission Research, Washington.
23. Singh, U., A. Bera, R. R. Rao, and A. K. Sinha, "Synthesized parameters of MIG for 200 kW, 42 GHz gyrotron," *Int. J. Infrared*

- Milli. Waves*, Vol. 31, 533–541, 2010.
24. Baird, J. M. and W. Lawson, “Magnetron injection gun (MIG) design for gyrotron applications,” *Int. J. Electronics*, Vol. 61, 953–967, 1986.
 25. Lawson, W., “MIG scaling,” *IEEE Trans. Plasma Sci.*, Vol. 16, 290–295, 1988.
 26. Hermannsfeldt, W. B., EGUN, Stanford University Report SLAC-226, Stanford Linear Accelerator Center, 1979.
 27. Singh, U., N. Kumar, N. Kumar, S. Tandon, H. Khatun, L. P. Purohit, and A. K. Sinha, “Numerical simulation of magnetron injection gun for 1 MW 120 GHz gyrotron,” *Progress In Electromagnetics Research Letters*, Vol. 16, 21–34, 2010.
 28. Kumar, N., M. K. Alaria, U. Singh, A. Bera, T. P. Singh, and A. K. Sinha, “Design of beam tunnel for 42 GHz, 200 kW gyrotron,” *Int. J. Infrared Milli. Waves*, Vol. 31, 601–607, 2010.
 29. Gantenbein, G., et al., “Experimental investigations and analysis of parasitic RF oscillations in high power gyrotrons,” *IEEE Trans. Plasma Sci.*, Vol. 38, 1168–1177, 2010.
 30. Nguyen, K., B. Danly, B. Levush, and M. Blank, “Electron gun and collector design for 94-GHz gyro amplifiers,” *IEEE Trans. Plasma Sci.*, Vol. 26, 799–813, 1998.
 31. Poonia, S., S. Tandon, U. Singh, and A. K. Sinha, “Design studies of collector for 42 GHz gyrotron,” *National Conference on Microwave, Antennas, Propagation and Remote Sensing*, Bhilwara, India, Dec. 19–21, 2008.
 32. Thumm, M., “Development of output power window for high power long pulse gyrotrons and EC wave applications,” *Int. J. Infrared Milli. Waves*, Vol. 19, 3–14, 1998.
 33. Heidinger, R., G. Dammertz, A. Meier, and M. Thumm, “CVD diamond windows studied with low and high power millimeter waves,” *IEEE Trans. Plasma Sci.*, Vol. 30, 800–807, 2002.
 34. CST-Microwave Studio, *User Manual: 2006 Version*, Darmstadt, Germany.